Journal of the European Ceramic Society **18** (1998) 1845–1855

PII: S0955-2219(98)00124-1
0955-2219/98/$—see front matter

Local Mechanical Characterisation and Modelling of the Interfacial Behaviour In Hi-Nicalon/BN/α-Si_3N_4 Ceramic Matrix Composites by Way of Instrumented Microindentation Tests

Monssef Drissi-Habti* and Kikuo Nakano

National Industrial Research Institute of Nagoya (NIRIN), Hirate-Cho Kita-Ku, Nagoya 462, Japan

Abstract

Microindentation tests (spherical indentation) have been used to evaluate local mechanical properties of Hi-Nicalon fibre reinforced silicon nitride ceramic matrix composite. This technique gave a satisfactory estimate of in-situ *longitudinal Young's modulus of both the matrix and the fibres which correlates quite well with 3-points bend tests. By means of the same technique, but with a different indenter (pyramidal), the interfacial behaviour has been studied. When varying the maximum applied load,* F_{max}*, and considering a constant interfacial shear stress, the presence of Poisson's effect has been detected. Based on Coulomb's law of friction, a model has been proposed to extract frictional stress values adjusted for Poisson's effect. The advantages of this model are the explicit integration of all contributions to the clamping stress at the fibre-matrix interface as well as the use of measured topography properties of Hi-Nicalon fibres.*

Keywords: CMCs, microindentation, atomic force microscope (AFM), Poisson's effect

1 Introduction

Ceramic matrix composites (CMCs) are still considered promising candidates for use at high temperatures, in oxidising atmospheres, mainly in the aerospace industry. However, despite some promising results obtained on well-established materials, CMC properties are not sufficient yet to be competitive.[1] This is mainly due to the sensitivity to oxidation of the available SiC-based fibres (owing to their high free oxygen and/or carbon content), as well as the ineffective protection against corrosion of the fibre-matrix interface. Recently, Nippon Carbon has processed a new ceramic fibre: Hi-Nicalon with less than 0·4% oxygen content. The achievement of this fibre can boost CMCs development.[2] In addition to processing problems, mechanical properties of CMCs must be evaluated on a large scale. Among mechanical tests which must be carried out, are those related to the evaluation of the effects of the processing route on (i) the mechanical properties of the matrix and the fibres and (ii) on the shear stress transfer at the fibre-matrix interface.

For the former, it was proven that the mechanical properties of the fibre and the matrix (in this system) are somewhat affected by processing parameters.[2] One of the most effective way to evaluate this problem is the use of continuous microindentation test records, which allow a local estimate of the longitudinal Young's modulus (see for example, Ref. 3), as well as the hardness of the fibres and the matrix. As a matter of fact, more comprehensive view of the performance of a composite, which is under development, can be gathered. This was achieved by comparing such results with the one's derived from as-received fibres and the monolithic matrix; and by coupling the same data base with the evolution of the microstructure of the composite. In this way, processing route conditions can be tailored and better CMCs performance can be achieved.

For the latter, it is well known that the thermomechanical performance of a CMC is strongly related to the thermomechanical behaviour of the

*To whom correspondence should be addressed.
e-mail: drissi@nirin.go.jp

fibre-matrix interface,[4] which is the key of the stress transfer from the matrix onto the fibres. To get an insight into the micromechanics of the interfacial behaviour, a variety of microindentation, pushing and pulling techniques including single and multiple fibres have been proposed. The goal is to understand how the load is transferred at the fibre-matrix interface, what are the main parameters governing this mechanism and to propose some tools for their direct estimate.[5–10] During microindentation tests, most of the analysis proposed to account for the interfacial behaviour assumed shear lag models with different levels of approximation. Mainly, all these analysis can be separated in two classes. The first one assumes a constant frictional stress, τ, at the fibre - matrix interface, reflected by a proportional relation between τ and the sliding length, L.[5–7] Whereas, the second class views the sliding stress at the fibre-matrix interface obeying to Coulomb's law of friction. This means that the frictional stress is directly proportional to the radial clamping stress at the fibre-matrix interface and that the coefficient of proportionality, μ, is a constant. However, the assumption of a constant frictional stress is neglecting the expansion of the fibre due to the so-called Poisson's effect. On the reverse, Coulomb's law of friction is taking into account this effect which adds to or subtracts from the radial clamping stress depending whether one is pushing (Fig. 1) or pulling the fibre. When Poisson's effect is of a high magnitude, its estimate becomes a key point when using microindentation test results for the purpose of modelling the crack opening micromechanism during fatigue tests.

The first part of this article will be devoted to the analysis of local mechanical properties of the matrix and the fibers, using *spherical indentation*. The second part will concern the modelling of the interfacial behaviour with the help of microindentation tests, performed using a *pyramidal microindenter*.

2 Materials and experiments

The investigated material is made up with Hi-Nicalon fibres, boron nitride coated. Details pertaining to the process route are given elsewhere.[2] Relevant physical data of the composite are listed in Table 1.[2] The topography of both virgin and coated Hi-Nicalon fibres were investigated using Atomic Force Microscope (AFM).[2] Multiple indentation tests were carried out using a spherical indenter (diamond ball) mounted on a completely automated force-driven static measuring ultra

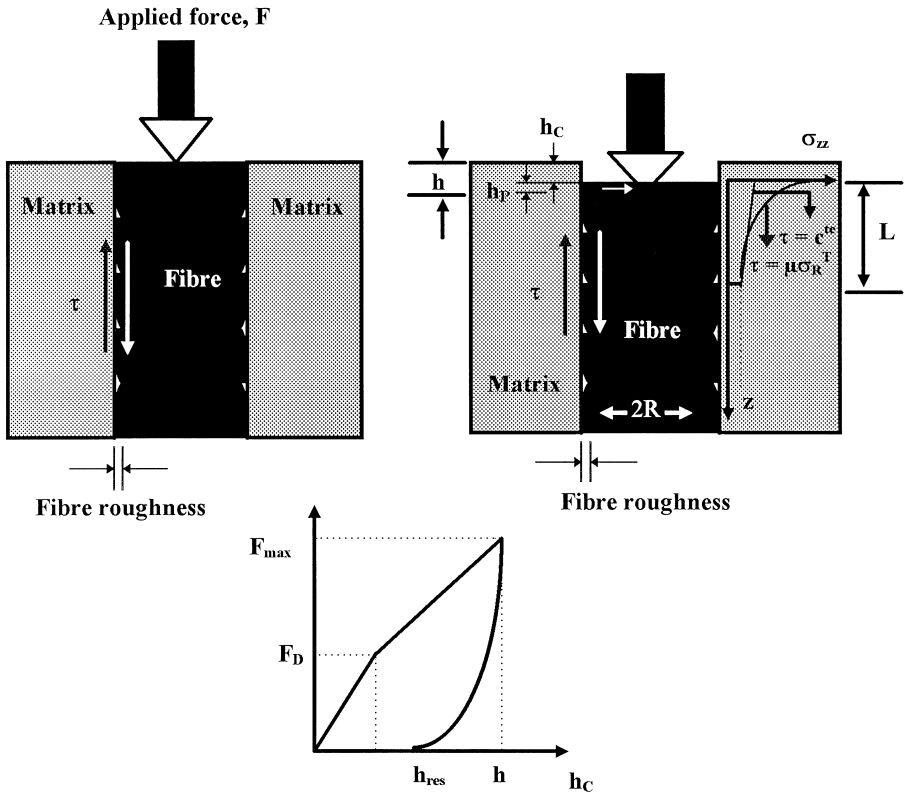

Fig. 1. Illustration of the unit cell consisting on a fibre surrounded by the matrix. The topography of the fibre is characterised by a roughness amplitude, A. When the microindentor pushes the fibre, the true displacement of the fibre, h_c is obtained by subtracting the microindentor penetration, h_p, from the total displacement, h, according to the analysis of Marshall and Oliver (1987).[6] The fibre debonding initiates at a load, F_D, and continues up to the maximum load under the combined effects of the elastic contraction of the fibre and the sliding. The debonded length dictates the sliding length, L.[11]

Table 1. Few physical data of the fibre, matrix and composite[2]

Fibre	$\alpha(\times 10^{-6}/°C)$	*Poisson ratio*	E_f *(GPa)*	σ_f *(MPa)*
Hi-Nicalon (Nippon carbon)	3·5 (0–550°)	0·15	250	1940
Matrix	α ($\times 10^{-6}$/°C)	Poisson ratio	E_m (GPa)	σ_m (MPa)
α–Si_3N_4	2·86 (0–550°)	0·28	193	538
The composite	V_m (%)	V_f (%)	Sintering temperature	Porosity (%)
Hi-Nicalon/BN/Si_3N_4	49	48	155°C	2·9

microindentation instrument (UMIS 2000).[2,12] For this part of the study, UMIS 2000 was equipped with a spherical indenter. The spherical indenter is a diamond cone (included angle of 60 or 90°), terminated with a radius in the range 2 to 50 μm. Tests were conducted on fine polished surfaces of specimens, previously embedded in resin. The fibre-matrix interfacial characterisation was performed on a Shimadzu DUH-50 testing machine with 0·5 N maximum load and a diamond cone angle indenter of 115°. Tests were force controlled and conducted at a loading speed of 1·3 mN s^{-1}.

3 Results and discussion

3.1 In-situ mechanical characterisation of the matrix and the fibres

3.1.1 Theory

Microindentation tests were performed on the fibres and the matrix (both on monolithic Si_3N_4 and on matrix rich-regions in the composite) with the scope to evaluate the local Young's modulus (LYM) of the matrix and the fibres. For such purpose, the multiple partial unloading procedure has been used.[2] Such tests are particularly suitable for a spherical indentation and give reliable measures of the LYM as a function of the depth of elastic/plastic penetration for materials whose properties vary with distance from the surface.[2] Before going to the presentation of the results, let us resume briefly the theory of spherical indentation, which will be applied in this work. Following Fig. 2, if a diamond ball (diameter D) is pushed into an elastic body, an initially elastic displacement (d) is recorded, and was expressed by Ref. 13 starting from Hertz's[15] solution of the Boussinesq problem:

$$d = (9/8)^{1/3} * (1/E_m)^{2/3} * (1/D)^{1/3} * F^{2/3} \qquad (1a)$$

where the longitudinal Young's modulus of the material (E_m) is given by:

$$1/E' = \left(1 - v_i^2\right)/E_i + \left(1 - v_m^2\right)/E_m \qquad (1b)$$

The longitudinal Young's modulus and the Poisson ratio of the diamond indenter are v_i and E_i and the Poisson ratio of the material is v_m. In our case, the spherical indenter is diamond made, hence the ratio $\left(1 - v_i^2\right)/E_i \approx 10^{-12}$. The mean pressure value, exerted on the material is given by the following relation:

$$P_m = F/\left(\pi^* a^2\right) \qquad (1c)$$

where a is the circle of contact at the ball–material interface, and is related to the displacement (d) and the radius R of the ball by the relation proposed by Ref. 16:

$$d = a^2/R \qquad (1d)$$

It should be noted that during loading, the mean pressure over the elastic mark will increase up to a stress value corresponding to the onset of local irreversible deformation. Starting from this stress level, any increase of load leads to a deformation value, which maintains the mean pressure equivalent to the yielding stress. One of the assumption is that the transition from the local elasto-plastic behaviour to the plastic behaviour is reached when the mean pressure equals the hardness (H) of the material. Setting $P_m = H$, combining eqns (1c) and and (1d) and using eqn (1a), the force corresponding to the transition from elasto-plastic to plastic behaviour is given by:

$$F_t = (\pi \mathrm{HRC})^3 * (1/\pi E_m)^* (1/D) \qquad (1e)$$

where C is a constant. At F_t, the radius of the contact circle is:

$$a_t = \sqrt{(F_t/\pi H)} \qquad (1f)$$

and the elastic displacement at the transition load is derived by analogy to eqn (1d):

$$d = a_t^2/R \qquad (1g)$$

At this step level, one important thing to note is that sphere-loading a material, up to the transition force (F_t), followed by unloading results in complete elastic response. Thus, the knowledge of two points along the unloading curve is enough to estimate h_r. When increasing the load further than F_t,

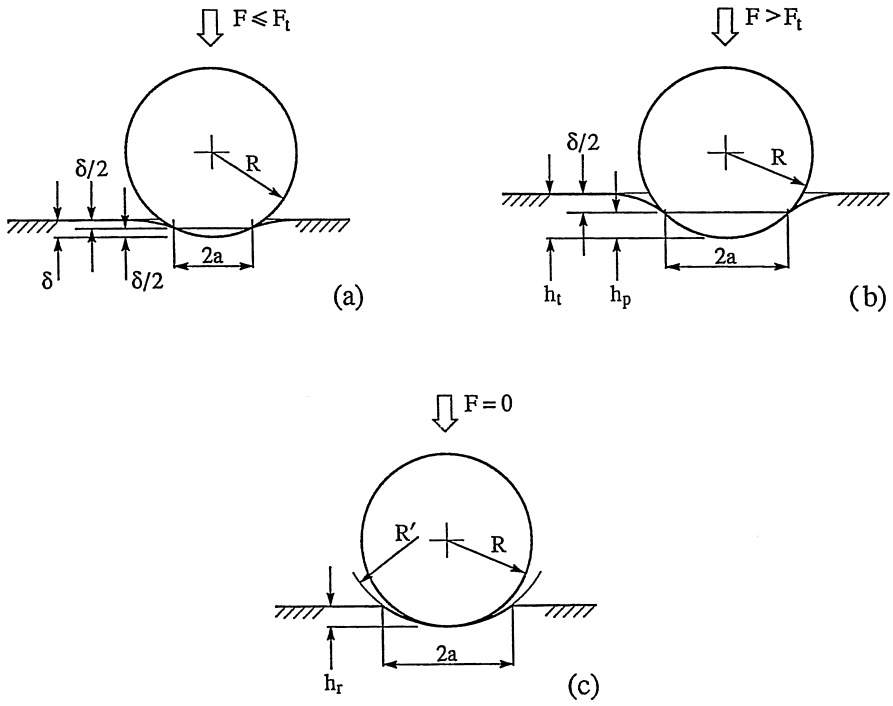

Fig. 2. Illustration of the spherical indentation test and the corresponding parameters.[14]

the indenter mark is widened following a local plastic deformation. Consequently, this small variation can lead to a variation in the onset of irreversible deformation. Therefore, the diameter of the indentation (M) is a function of Meyer's index (m), C and F:

$$M = 2 \times a = C \times F^{1/m} \tag{1h}$$

Note that Meyer's index has been taken to be $x + 2$ by Tabor,[17], where x is the strain index of the material. Typically, x varies between 0 (for likely plastic solids) to 0·6 (for elasto-plastic materials). The parameter M_t (corresponding to the diameter of the indentation, at the transition load) is therefore useful to calculate the contact circle radius (a') for a load value (F') higher than F_t, as:

$$a' = 0{\cdot}5 \times M_t \times (F'/F_t)^{1/m} \tag{1i}$$

The depth of penetration below the circle of contact (h_p) at loads higher than F_t is given from simple geometrical considerations as:

$$h_p = R - \sqrt{(R^2 - a'^2)} \tag{1j}$$

The residual penetration (h_r) which is not taken into account by the elastic deflection as well as the radius of the depression are given by:

$$h_r = h_p - d/2 \tag{1k}$$

and

$$R' = (a^2 + h_r^2)/2h_r \tag{1l}$$

Note that h_r is assumed to be the depth of recovered surface depression. The elastic displacement (d) is therefore needed to estimate further displacement following next loading increment. This procedure is repeated and in this way, the depth of penetration at each load increment is calculated until the maximum load is reached. The total depth measured at each increment is given by the following relation:

$$h_t = h_r + d \tag{1m}$$

Starting from the method described above, which has also been applied to the characterisation of thin solid films by Refs 14,18, the load/unload procedure for the extraction of the LYM is hereafter briefly described. In the multiple partial unloading (20 in our case), a single indentation is partially unloaded in one increment at each step by an amount of 50% of the total step. Each force step provides two pieces of information: the total depth of elastic/plastic penetration and a measure of the recovery from that load. The analysis of the partial unload data (see above) provides for the extraction of the LYM at each step[2], using eqn (1b). Two points must however permanently kept in mind. The first one is to devoid any shock when contacting the material. This can be achieved by carefully selecting the low contact load speed of the indenter. The second point is the suitable selection of the maximum applied load. Indeed, care must be given to devoid maximum load values which can introduce microcracking into the material. In such cases, the results are depending on the amount of

damage introduced, as pointed out by Cook and Pharr.[19] Still related to instrumented indentation, one might also point out the work of Loubet *et al.*[20] on MgO monocrystals. These authors illustrated all the parameters which are intervening in the analysis of load-displacement relationships. Their analysis, based on the assumption that the unloading part is not linear,[21] requires fitting a tangent to the upper portion of the unloading curve, using the elastic punch theory,[22] to estimate the penetration depth.

Microindentation results recorded for the monolithic matrix and the matrix rich-regions in the composite, are depicted in Fig. 3(a). As noticed, both local LYM values, plotted as a function of the depth below penetration, show a similar constant value of 193 GPa, attained after a penetration of about 100 nm (matrix Poisson's ratio (ν_m) being 0·28). Despite the small scatter, this value is in good agreement with flexure test results.[2]

The averaged variation of the LYM as a function of penetration depth, as derived from indentation tests performed on Hi-Nicalon fibres in the composite (up to $F_{max} = 250$ mN) are plotted in Fig. 3(b). A constant value of 106 GPa of the LYM is reached after a penetration of about 180 mn. In both cases, we should keep in mind that during the first load/unload cycles (Fig. 4), the local plastic behaviour under the indenter is not yet achieved. Hence, the slope of the unloading part is very sharp and the value of the LYM is overestimated. When the applied load exceeds the transition force (F_t), the local plastic behaviour takes place and the elastic response upon unloading leads to the right estimate of the LYM, reflected by a plateau value.

According to mechanical test results and Atomic Force Microscope observations, this low value of E_f has been attributed to the effects of both the fibre's BN-coating and the hot-pressing stages.[2,12] For the former, it was shown from a deep comparison between virgin and BN-coated fibres that the coating by boron nitride did affect the external surface of Hi-Nicalon. Such effects arise in general when the atmosphere of the coating stage is not rigorously controlled and a small amount of oxygen remains. However, provided that the surface alteration is not enough to lower drastically the LYM of the composite, the effects of hot pressing stage (the latter) have been proposed as an additional source of troubles.

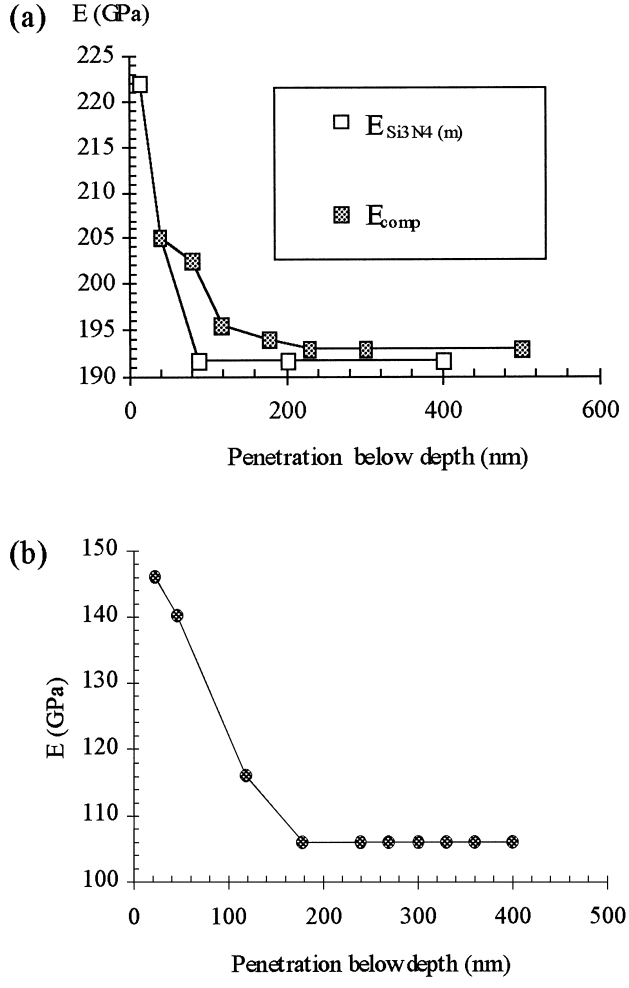

Fig. 3. (a) Mean evolution of the longitudinal Young's modulus values as a function of the penetration below contact when indenting the monolithic silicon nitride ($E_{Si_3N_4(m)}$) and the matrix rich regions in the Hi-Nicalon/BN/silicon nitride composite (E_{comp}). The maximum applied force is 250 mN; (b) evolution of the longitudinal Young's modulus as a function of the penetration below contact of the BN-coated Hi-Nicalon fibres using microindentation tests. Ale maximum applied force is 250 mN.[12]

3.2 Modelling of the shear stress transfer at the fibre-matrix interface

3.2.1 Theory

We will consider the unit cell composed by a ceramic matrix surrounding an axially loaded fibre, with a radius R (Fig. 1). The interfacial bonding between the fibre and the matrix is considered weak enough so that debonding is initiated in a stable way. Under such conditions, when the load carried by the fibre is sufficiently high, fibre-matrix debonding initiates at a stress level σ_D:

$$\sigma_D = F_D/\pi R^2 \tag{2}$$

Based on an energy analysis which takes into account residual stresses, Marshall *et al.*[6] have shown that the debond stress is related to the debond energy, G_D, and the axial residual stress in the fibre, σ_f^{res}:

$$\sigma_D - \sigma_f^{res} = \sqrt{\left(4E_f G_D/R\right)} \tag{3}$$

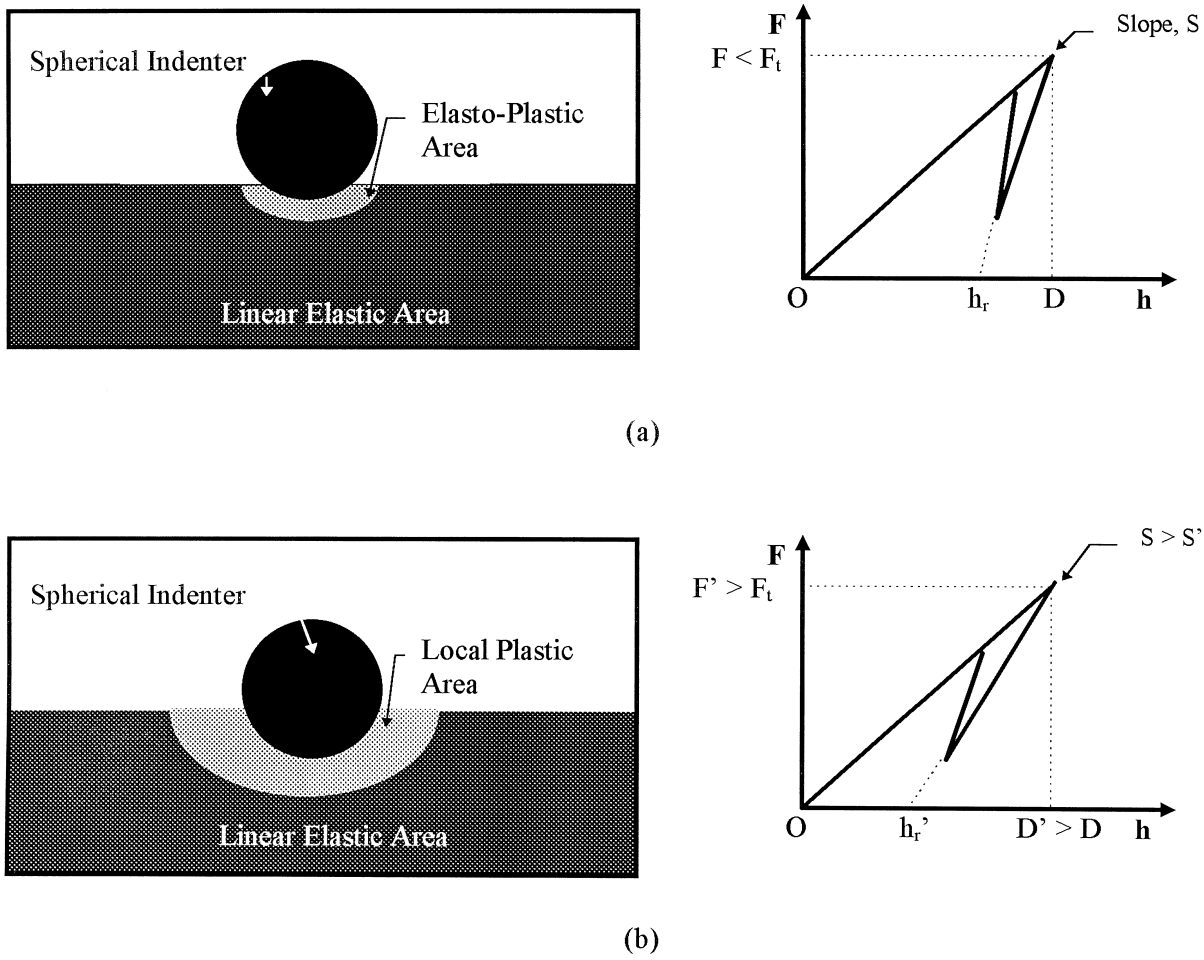

Fig. 4. Illustration of the load–displacement relationship in instrumented microindentation tests, in conjunction with the development of the elasto-plastic area around the indentation mark. (a) When loading a polished surface of the material up to a maximum force (A), well below the transition force, F_t, an elasto-plastic area grows up. At this stage, when partly unloading the specimen, the longitudinal Young's Modulus (LYM) is overestimated. (b) When the elasto-plastic zone is fully developed (above F_t), the partial unloading cycle leads to an elastic response of the material from which the true estimate of the LYM can be gathered.

This relation is given in the case where the interfacial crack length is at least greater than three times the fibre radius. The residual stress within the fibre, σ_f^{res} can be evaluated by load cycling the fibre and analysing quantitatively the amount of recovery when the load is relaxed (h is the displacement of the fibre; Fig. 1):

$$\sigma_f^{res} = \left(F_{max}/2\pi R^2\right) \times [1 - (h_{res}/(h_{max} - h_{res})] \quad (4)$$

Available models of the interfacial sliding start from the assumption of either (i) a constant frictional stress (for both debonded and weakly bonded interface) or (ii) Coulomb's law of friction. The trends derived from these two assumptions are summarised below as well as the theoretical basis of our model of the shear stress transfer at the fibre-matrix interface.

3.2.1.1. Constant frictional stress. In the case of debonded interfaces, the fibre is subjected to the axial stress, σ, which is resisted by a constant shear stress, τ, acting only on the external surface of the fibre. If the shear stress exceeds τ, then fibre-matrix sliding occurs. Hence, the mechanical equilibrium of the fibre, for distances less than the sliding length, requires that:

$$d\sigma/dz = -2\tau/R \quad (5)$$

The fibre slides relatively to the matrix at a constant shear stress, τ, along a distance L, derived from the integration of expression (5) with regards to boundary conditions (i.e. $\sigma = F/\pi R^2$ at $z = 0$ and $\sigma = 0$ beyond the sliding distance, L):

$$L = F/2\pi R\tau \quad (6)$$

and the strain at any section of the fibre along z axis is given by:

$$\varepsilon_z = \left(F/\pi R^2 E_f\right) \times (1 - z/L) \quad (7)$$

Generally, where the interface is weakly bonded, the sliding length is dictated by the debond crack

length. Then, the displacement of the fibre can be obtained from the integration of eqn (5) between 0 and the debond length. Marshall[5,6] has proposed the following expression relating the real displacement of the fibre, h_c, to the applied force, F, and the debond energy, $\Gamma(G_D = 2\Gamma)$:

$$h_c = (F^2/4\pi R^3 \tau E_f) - (2\Gamma/\tau) \quad (8)$$

3.2.1.2. Coulomb's law of friction. Let us consider a ceramic fibre, subjected to an axial compressive stress. In this case, a radial compressive stress is generated at the interface due to Poisson's effect, which in turn, modifies the resulting interfacial radial stress. Therefore, Marshall's analysis becomes inappropriate for modelling the shear stress transfer. To account for Poisson's effect, a more rigorous analysis would assume the frictional stress obeying Coulomb's law of friction and would take into account all the contributions due to the clamping stress at the fibre-matrix interface. For this purpose, the micromechanisms at the origin of the frictional stress must be analysed.

When ignoring fibre roughness effects, the sliding stress had been expressed by Ref. 9:

$$\tau = \tau_0 - \mu\sigma_R \quad (9)$$

where τ is the sliding resistance, μ the coefficient of friction, σ_R the compressive stress normal to the interface due to thermal and processing induced residual stresses and τ_0 the constant sliding stress.

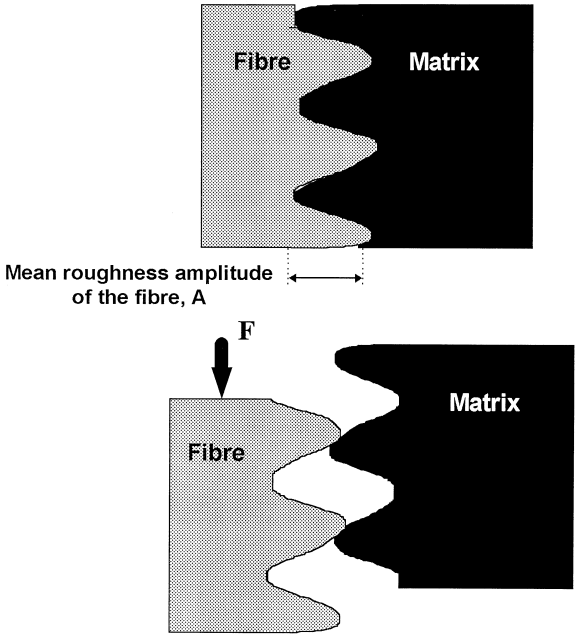

Fig. 5. Illustration of the initial state of the fibre-matrix interface, characterised by a correlation between asperities. When the fibre is pushed down, the asperities debond and this leads to the stress, σ_R^{RA}, which adds to the clamping stress at the fibre-matrix interface.

In a given CMC, the original position of the interface is in fact characterised by a geometrical correlation between the asperities of the fibre and the matrix (Fig. 5). Once removed from their initial position, the asperities of the fibre decorrelate and generate, in the case of indentation tests, an additional compressive stress, which must be added to the thermal radial residual stress. Thus, the radial pressure induced by the roughness determines *mechanistically* τ_0 such that τ [eqn (9)] becomes entirely *Coulombian*:[23]

$$\tau = \mu\sigma_R^T \quad (10)$$

where σ_R^T is the total clamping stress at the fibre matrix interface. In the general case considered herein, this clamping stress, σ_R^T, originates from three contributions: the roughness induced compressive stress, σ_R^{RA}, residual stresses, σ_R^{TRS} and the stress σ_R^{PE} which arises from the expansion of the fibre under the applied stress, σ, following Poisson's effect:

$$\sigma_R^T = \sigma_R^{RA} + \sigma_R^{TRS} + \sigma_R^{PE} \quad (11)$$

When the case of a single filament is considered ($V_f = 0$) and under some assumptions, Kerans and Parthasaraty[24] expressed the contributions of thermal residual stress (σ_R^{TRS}) and roughness amplitude (σ_R^{RA}) to the clamping stress, σ_R^T, as:

$$\sigma_R^{TRS} = C \times (\alpha_m - \alpha_f) \times T \quad (12)$$

and

$$\sigma_R^{RA} = C \times (-A/R) \quad (13)$$

where α_m and α_f are the coefficients of thermal expansion of the matrix and the fibre, respectively, A is the roughness amplitude of the fibre (Fig. 1), ΔT is the difference between room temperature and the temperature corresponding to a residual stress free state and C is a function of the elastic constants of the fibre and the matrix. In the general case considered in this work, C is given by the following expression:

$$C = E_m E_f / [E_f(1 + \nu_m) + E_m(1 - \nu_f)] \quad (14)$$

During push-down tests, fibre's expansion due to Poisson's effect arises from the difference between the longitudinal strain on the fibre (ε_{lf}^{PE}) and on the matrix (ε_{lm}^{PE}), added to the fact that Poisson's ratio of the fibre (ν_f) is different from that of the matrix (ν_m). This mismatch leads to the following radial stress which adds to the radial clamping stress in the case of push-in tests:

$$\sigma_R^{PE} = C \times \left(\varepsilon_{lm}^{PE} - \varepsilon_{lf}^{PE}\right) \quad (15)$$

When the fibre is pushed in, the longitudinal stress in the matrix is negligible and the expansion of the fibre, ε_{lf}^{PE}, is a function of the compressive stress within the fibre (α), the longitudinal Young's modulus (E_f), and the Poisson ratio of the fibre (v_f). It follows therefore that:

$$\varepsilon_{lf}^{PE} = -v_f\sigma/E_f \quad (16)$$

By substituting eqn (15) into eqn (14), the contribution σ_R^{PE} can be expressed as a function of the compressive stress within the fibre and the elastic constants of the fibre and the matrix:

$$\sigma_R^{PE} = -v_f C\sigma/E_f \quad (17)$$

The compressive stress within the fibre, σ, can be calculated when supposing it to be entirely balanced by the frictional stress. Then, the equilibrium conditions in any section of the fibre (along the z axis) impose that the variation of the axial compressive stress is completely accommodated by the frictional stress $\tau\left(\tau = \mu\sigma_R^T\right)$:

$$-\pi R^2 * \left(d\sigma/dz\right) = 2\pi R^* \mu\sigma_R^T \quad (18)$$

Combining eqns (11),(17),(18), and integrating, we obtain the following expression for the axial applied stress in the fibre, σ:

$$\sigma = 1/C' \times \left[\left(\sigma_R^{TRS} + \sigma_R^{RA} + C' \times \sigma_m\right) \times \exp(-2\mu C' z/R) - \left(\sigma_R^{TRS} + \sigma_R^{RA}\right)\right] \quad (19)$$

where σ_m is the uniform applied pressure on the top of the fibre and C' is the quantity $-v_f\, C/E_f$. By integrating the applied strain in the loading direction (according to the way of integration of Ref. 9, the displacement of the top of the fibre, $h_c\left(h_c = h - h_p\right.$; Fig. 1) under the applied force, F, can be simulated using the following relation:

$$h_c = \left[(1 - 2v_f C)/2\mu CR\pi E_f\right] \times F - \left[R \times (1 - 2v_f C) \times \left(\sigma_R^{TRS} + \sigma_R^{RA}\right)/2\mu C^2 E_f\right] \times \mathrm{Ln}\left[1 + C \times F/\pi R^2\left(\sigma_R^{TRS} + \sigma_R^{RA}\right)\right] \quad (20)$$

Therefore, when the values of R and F, are known, the coefficient of friction, μ, can be varied to fit the loading part of load–displacement relationships. Hereafter, we will use these trends to analyse the shear stress transfer.

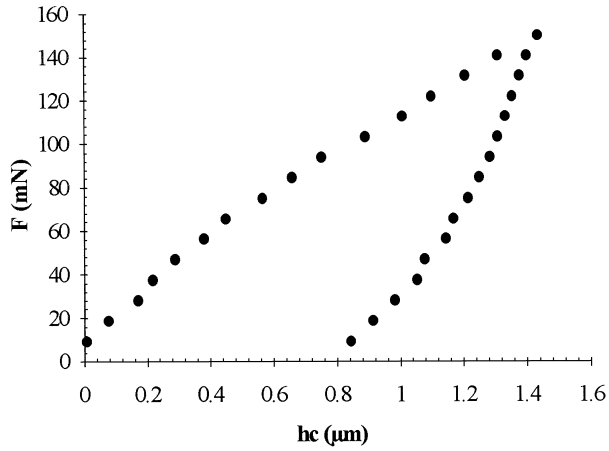

Fig. 6. A typical load–displacement relationship obtained by loading up to an applied force, $F_{max} = 150$ mN, a fibre with a radius $R = 7{\cdot}5$ μm.[11]

3.2.2 Load–displacement relationships ($F-h_c$)

A typical $F - h_c$ curve is presented in Fig. 6. The loading part is slightly curved as for most of F–h curves, and this prohibits a blind transposition of Marshall's model to our results. A low debonding stress is calculated [340 MPa using eqn (2)]. Using eqn (4) and assuming the conditions of Ref. 6, the axial residual stress, is $\sigma_f^{res} = -35$ MPa. The fibres in this composite are under a low magnitude residual compressive stress. The unloading part shows a recovery, $h_{res} = 0{\cdot}75$ μm, whereas the maximum displacement is $h_{max} = 1{\cdot}434$ μm. This leads to a ratio, $h_{res}/h_{max} = 0{\cdot}523$. Based on the analysis of Ref. 6, residual stresses lead to a relative amount of recovery higher than 0·5 for tensile stresses and smaller than 0·5 for compressive residual stresses within the fibres. Hence, the ratio of 0·523 deduced corresponds well with the low compressive residual stress value of −35 MPa calculated in Hi-Nicalon fibre composite. The debonding energy G_D 0·03 J m^{-2}, is much lower than in the case of unidirectional SiC–SiC composite (2 J m^{-2}, Ref. 25) but is similar to the case of SiC–LAS composite (0·37 J m^{-2}, with turbostratic carbon interphase[26]). The difference between these values highlights the effect of the sign and the magnitude of residual stresses.

3.2.3 Effects of varying F_{max}

The sliding stress is often calculated assuming that the interfacial shear stress is uniform.[5,6] This assumption fits well with a low magnitude coefficient of friction composites. For several cases, the expansion of the fibre due to Poisson's effect increases the radial clamping stress and leads to the variation of the frictional stress along the sliding length. When making a parallel, Marshall's analysis can be viewed as a particular case of Coulomb's law of friction.

During indentation tests, when increasing F_{max} the contact area between the fibre and the matrix

increases. In the event Poisson's effect exists, an increase in the frictional stress is expected. To check whether the frictional stress in Hi-Nicalon fibre reinforced silicon nitride composites is affected by Poisson's effect, microindentation tests were performed at different applied force: 150, 200 and 250 mN and the mean values of τ, calculated using the model of Ref. 6 are plotted in Fig. 7 as a function of the fibre radius. It should be noted that for every fibre radius, seven tests were done and the averaged values are considered in Fig. 7. As shown, τ values are close as long as the fibre radius is higher than 10 μm. For smaller fibre radius, τ values calculated from tests performed with $F_{max} = 150$ mN are smaller than that evaluated for higher F_{max}. The difference range is small (typically 1–3 MPa), which is a typical manifestation of Poisson's effect. A micromechanical analysis is proposed hereafter to separate the contribution of the expansion of the fibre from the frictional stress.[11]

The compressive stress due to the roughness amplitude (A) of the fibres, σ_R^{RA}, can be estimated when the roughness amplitude of the fibres is known. Using an Atomic Force Microscope (AFM), A has been estimated as 15 mn.[11] Following, the quantities σ_R^{RA} and σ_R^{TRS} are calculated using eqns (12–14). Thereafter, using eqn (20) as well as the values of σ_R^{RA} and σ_R^{TRS}, the loading parts of $F - h_c$ curves will be fitted by varying the coefficient of friction, μ. With the appropriate value of μ deduced from the fitting procedure, τ will be calculated using expressions (10) and (11), by setting at first $\sigma_R^{PE} = 0$. This first assumption will let us have an idea about the magnitude of the frictional stress when ignoring the expansion of the fibre. As a second step, the maximum contribution of Poisson's effect will be considered in order to get the extremal range of variation of the frictional stress when including this effect.

3.2.4 Evaluation of the coefficient of fiction, μ

With the help of the mean value of A, the parameters of Table 1, the longitudinal Young's modulus of fibres in the composites (we will use the true value: $E_f = 106$ GPa[12] since it reflects the actual state of the fibres inside the composite) and using eqns (12) and (13), the roughness amplitude contribution to the clamping stress is calculated as a function of the fibre radius. With $R = 7{\cdot}5$ μm, σ_R^{RA} is $-136{\cdot}5$ MPa. Using eqns (11) and (13), the residual stress contribution to the clamping stress (σ_R^{TRS}) is 24 MPa. The fitting procedure of $F - h_c$ relationships [using eqn (19)] is illustrated in Figs 8 and 9. for two fibres with the same radius (7·5 μm) up to $F_{max} = 150$ and 200 mN. The derived μ values of 0·03 and 0·047 provide close fitting to experimental results for $F_{max} = 150$ and 200 mN, respectively.

Therefore, the frictional stress can be derived by way of Coulomb's law of friction, and restricting the clamping stress to the roughness of the fibre and thermal residual stresses contributions. Thereafter, the contribution of Poisson's effect will be calculated using eqn (16) with the stress of the fibre being equal to the maximum value attained at F_{max}.

Frictional stress values, ignoring Poisson's Effect ($\tau(PE = 0)$, data 1), the Maximal Contribution of Poisson's Effect (MPEC, data 2) and the summation of the two sets of values (Tau (PE = 0) + MPEC, data 3) are depicted in Fig. 10 as functions of the fibre radius. The results summarised in this figure are those obtained when pushing the fibres until $F_{max} = 150$ mN. It can be seen that data 1 values range between 8·8 and 4·3 MPa for $R = 5$ to 12 μm. In the same range of fibre sizes, data 2 varies

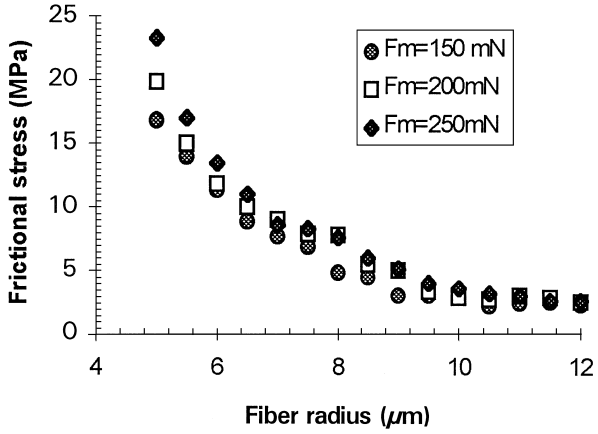

Fig. 7. Frictional stress calculated using the model of Ref. 6 for three different $F_{max} = 150$, 200 and 250 mN and plotted as a function of the fibre radius. As shown, τ values increase with increasing F_{max}.[11]

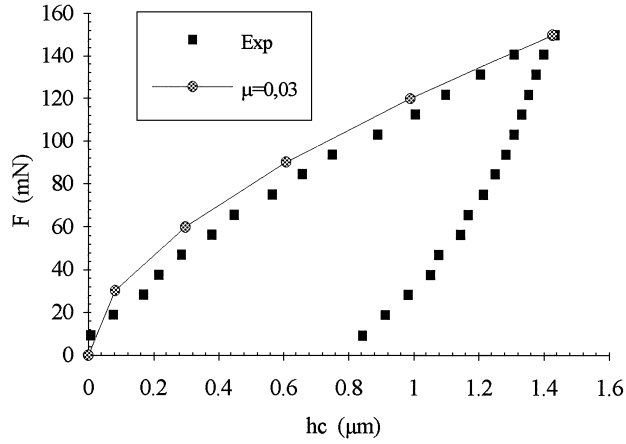

Fig. 8. Load – fibre displacement relationships (Exp) for a fibre radius $R = 7{\cdot}5$ μm loaded until a maximum force value of 150 mN, plotted along with the simulated one using expression (19) with a friction coefficient $\mu = 0{\cdot}03$.[11]

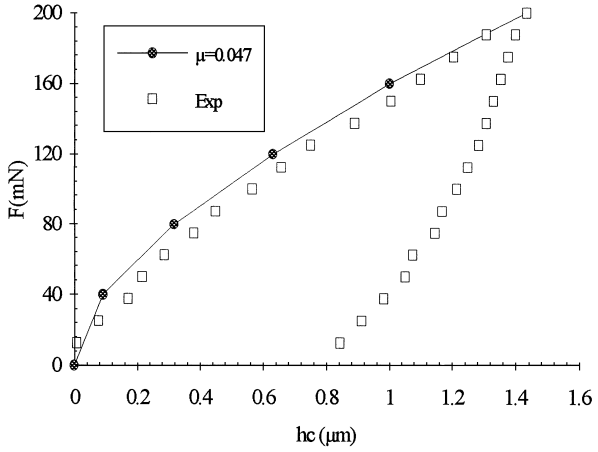

Fig. 9. $F - h_c$ (Exp) for a fibre radius $R = 7{\cdot}5\ \mu$m loaded until $F_{max} = 200$ mN, plotted along with the simulated one using expression (19) with a friction coefficient $\mu = 0{\cdot}047$.[11]

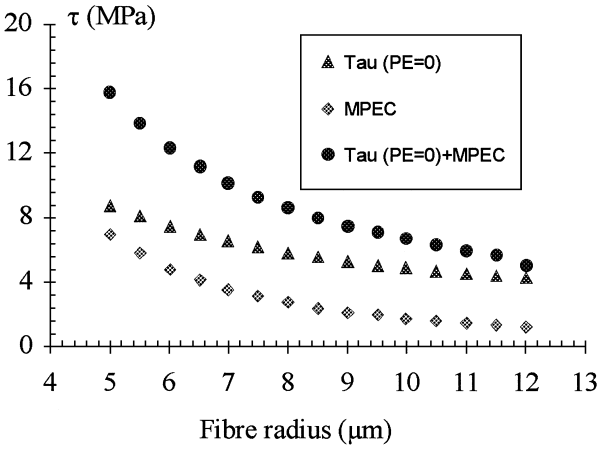

Fig. 10. Frictional stress values, τ, calculated using eqns (9) and (10) when ignoring Poisson's effect [τ(PE = 0)], the maximum Poisson's effect contribution (MPEC) and τ taking into account all contributions to the radial compressive stress [τ(PE = 0) + MPEC].[11]

between 7 and 1·2 MPa. The analysis of these results leads to two main points:

- For smaller fibre radius ($R = 5$ to $7{\cdot}5\ \mu$m), data 2 values (MPEC) are as high as the frictional stress due to both the roughness amplitude and thermal residual stresses.
- The MPEC decreases quickly within the range of fibre radius from 5 to 10 μm and slows down further at a low value, close to 1·2 MPa.

In this composite, most of the fibres have radius under 10 μm, as derived from numerous optical observations. Therefore, it comes that Poisson's effect must be taken into account when modelling the shear stress transfer in this composite. This special point emphasises the importance of determining the statistical fibre radius distribution.

4 Conclusions

Microindentation tests have been used to evaluate the mechanical properties of the matrix and the fibres inside the composite as well as to get an insight into the interfacial behaviour of Hi-Nicalon fibre reinforced silicon nitride ceramic matrix composite.

Spherical indentation tests results show that the fibres suffered from the processing stage. This technique as well as the analysis proposed shows that spherical microindentation tests are very suitable to estimate the *in-situ* mechanical properties of the fibre and the matrix. The method is promising, especially on a laboratory scale (during the development stage of the material), where only small size specimens are available and quick results are needed.

The interfacial behaviour of this composite has also been probed by way of a pyramidal microindentor. When assuming a constant frictional stress and performing microindentation tests for a range of maximum applied force, the existence of Poisson's effect has been shown. To adjust frictional stress values of Poisson's effect, a model, based on Coulomb's law of friction, has been proposed. The advantage of this model is the explicit integration into the clamping stress of all contributions (thermal residual stresses, roughness amplitude of the fibres and Poisson's effect). Starting from the equilibrium conditions, the loading parts of $F - h_c$ curves have been fitted by varying the coefficient of friction. Results show that Poisson's effect is of a high magnitude for fibre radius less than 10 μm.

The model proposed herein assumes that the load is a uniform pressure applied on the top surface of the fibres. Hence, one of the possible implication of this work would turn one's attention to check the degree of veracity of this assumption, as well as the effects of neighbouring fibres. Recent work on the fibre bundle push-out tests have clearly shown that the proximity of fibres leads to an additional constraint which restricts interfacial sliding.[27]. Hsueh[28] has partly taken into account the effects of neighbouring fibres (by introducing the V_f in the calculation of the C parameter), but this leads to dense calculations.

Acknowledgements

The authors would thank deeply the Science and Technology Agency (STA) and JSTEC of Japan for the financial support of this work.

References

1. Lamicq, P. and Choury, D., Ceramic matrix composite parts design, AGARD Workshop, Introduction of Ceramics into Aerospace Structural Composites, Antalya, Turkey, 1993, pp. 12–1–12–12.
2. Drissi-Habti, M. and Nakano, K., Assessment of the microstructure and the mechanical characteristics of the Hi-Nicalon fibers reinforced α = silicon nitride ceramic matrix composites. *Composites Sciences and Technology*, 1997, **57**(11), 1483–1489.
3. Parlier M., Passilly, B. and Sudre, O., AGARD Workshop, Introduction of Ceramics into Aerospace Structural Composites, Antalya, Turkey, 1993, pp. 5–1–5–8.
4. Naslain, R., Fiber-matrix interphases and interfaces in ceramic matrix composites processed by CVI. *Composite Interfaces*, 1993, **1**(3), 253–286.
5. Marshall, D. B., An indentation method for measuring matrix/fiber frictional stresses in ceramic composites. *J. Am. Ceram. Soc.*, 1984, **67**(12), C259.
6. Marshall, D. B. and Oliver, W. C., Measurement of interfacial mechanical properties in fiber-reinforced ceramic composites.. *J. Amer. Ceram. Soc.*, 1987, **70**(8), 542–548.
7. Marshall, D. B. and Oliver, W. C., An indentation method for measuring residual stresses in fiber-reinforced ceramics.. *Mater. Sci. Eng.*, 1990, **A126**, 95–103.
8. Marshall, D. B., Analysis of fiber debonding and sliding experiments in brittle matrix composites. *Acta Metall. Mater.*, 1992, **3**, 427–444.
9. Shetty, D. K., Shear-lag analysis of fiber push-out (indentation) tests for measuring interfacial friction stress in ceramic-matrix composites.. *J. Am. Ceram. Soc.*, 1988, **71**(2), C107.
10. Hutchinson, J. W. and Jensen, M. H., Models of fiber debonding and pull-out in brittle composites with friction.. *Mechanics of Materials*, 1990, **9**, 139–163.
11. Drissi-Habti, M. and Nakano, K., Modelling of the shear stress transfer in the Hi-Nicalon fiber reinforced α-silicon nitride ceramic matrix composite using microindentation tests.. *Comp. Sci. Tech.*, 1997, **57**(11), 1483–1489.
12. Drissi-Habti, M. and Nakano, K. Local mechanical characterization of the Hi-Nicalon fiber reinforced α-silicon nitride ceramic matrix composite using microindentation tests. In: *Key Engineering Materials*, ed. Daniel *et al.*, Vols. 127–131, 1997, 807–814. Trans Tech. Publications, Switzerland, 1997, pp. 807–814.
13. Hertz, H., *J. Reine Angew. Math.*, 1881, **92**, 156.
14. Swain, M. V. and Mencik, J., Mechanical property characterization of thin film using spherical tipped indenters. *Thin Solid Films*, 1994, **253**, 204–211.
15. Puttock, M. J. and Thwaite, E. G., Elastic compression of spheres and cylinders at point and line contact. CSIRO Internal Report, Melbourne, Australia, 1969.
16. Johnson, K. L., *J. Mech. Phys. Solids*, 1970, **18**, 115–126.
17. Tabor, D., *The Hardness of Metals*. Clarendon Press, Oxford, 1951.
18. Field, J. S., and Swain, M. V., *J. Mater. Res.*, 1993, **8**, 137.
19. Cook, R. F. and Pharr, G. M., Direct observation analysis of indentation cracking in glasses and ceramics. *J. Amer. Ceram. Soc.*, 1990, **73**(4), 787–817.
20. Loubet, J. L., Georges, J. M., Marchesini, O. and Meille, G., Vickers indentation curves of magnesium oxide (MgO). *Trans. of ASME, Journal of Tribology*, 1984, **106**, 43–48.
21. Shorshorov, M. K. H., Bulyshev, S. I. and Alekhin, V. P., Work of plastic and elastic deformation during indenter indentation. *Sov. Phys.Dokl*, 1981, **26**, 767–771.
22. Sneddon, L. N., The relation between load and penetration in the axisymetric Boussinesq problem. *Int. J. Eng. Sci.*, 1965, **1**, 47–52.
23. Mackin, T. J., Warren, P. D. and Evans, A. G., Effects of fiber roughness on interface sliding in composites. *Acta Metall. Mater.*, 1992, **40**(6), 1251–1257.
24. Kerans, R. and Parthasarathy, T. A., Theoretical analysis of the fiber pull-out and push-out tests. *J. Amer. Ceram. Soc.*, 1992, **74**(7), 1251–1257.
25. Evans, A. G., Ceramic matrix composites: challenges and opportunities. Workshop, Introduction of Ceramics into Aerospace Structural Composites, AGARD Conference, Antalya, Turkey, April 1993, 2–1–2–13.
26. Weihs, T. P. and Nix, W. D., Experimental examination of the push-down technique for measuring the sliding resistance of silicon carbide fibers in a ceramic matrix.. *J. Am. Ceram. Soc.*, 1991, **74**(3), 524–534.
27. Zhou, L. M. and Mai, Y. W., Analysis of fiber frictional sliding in fiber bundle push-out test.. *J. Am. Ceram. Soc.*, 1996, **77**(8), 2076–2080.
28. Hsueh, H. C., Evaluation of interfacial properties of fiber-reinforced ceramic composite using a mechanical properties microprobe. *J. Am. Ceram. Soc.*, 1993, **76**(12), 3041–3048.